ACS Photonics

Article

pubs.acs.org/journal/apchd5

Deterministic Approach to Achieve Broadband Polarization-Independent Diffusive Scatterings Based on Metasurfaces

He-Xiu Xu,[*,†,‡,§] Shaojie Ma,[†] Xiaohui Ling,[†,§] Xiao-Kuan Zhang,[‡] Shiwei Tang,[∥] Tong Cai,[†,‡] Shulin Sun,[⊥] Qiong He,[†,#] and Lei Zhou[*,†,#]

[†]State Key Laboratory of Surface Physics, Key Laboratory of Micro and Nano Photonic Structures (Ministry of Education) and Physics Department, Fudan University, Shanghai 200433, China

[‡]Air and Missile Defense College, Air Force Engineering University, Xi'an, 710051, China

[⊥]Shanghai Engineering Research Center of Ultra-Precision Optical Manufacturing, Green Photonics and Department of Optical Science and Engineering, Fudan University, Shanghai 200433, China

[#]Collaborative Innovation Center of Advanced Microstructures, Fudan University, Shanghai 200433, China

[∥]Department of Physics, Faculty of Science, Ningbo University, Ningbo 315211, China

[§]College of Physics and Electronic Engineering, Hengyang Normal University, Hengyang 421002, China

Supporting Information

ABSTRACT: Diffusive scatterings of electromagnetic (EM) waves by a thin screen are important in many applications, but available approaches cannot ensure uniform angular distributions of low-intensity scatterings without time-consuming optimizations. Here, we propose a robust and deterministic approach to design metasurfaces to achieve polarization-independent diffusive scatterings of EM waves within an ultrabroad frequency band and for wide-range of incident angles. Our key idea is to use high-efficiency Pancharatnam−Berry meta-atoms to form subarrays exhibiting focusing reflection-phase profiles, that can guarantee nearly uniform diffusive scatterings for arbitrarily polarized EM waves. As an illustration, we design and fabricate two metasurfaces and experimentally characterize their wave-diffusion properties in C, X, and Ku bands. Theoretical, numerical and experimental results demonstrate that our approach can diffuse the incident energy much more uniformly than available approaches based on the uniform-phase subarrays, thanks to the intrinsic wave-diffusion capabilities of the focusing-phase subarrays. The −7 dB fractional bandwidth is measured as 88.3% and the diffusive scattering behavior can be preserved up to 60° off-normal incidence irrespective of incident polarizations. Our approach, simple and robust, can help realize stealth applications under bistatic detections.

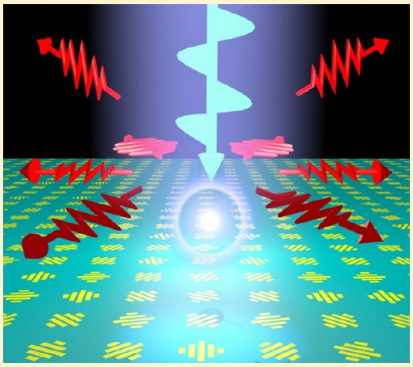

KEYWORDS: *broadband, diffusive scattering, focusing-phase, metasurface, Pancharatnam−Berry phase*

Invisibility and cloaking have intrigued a long-held interest due to the pressing demand on stealth and antistealth applications. Various strategies have been proposed and extensively studied in the past decades, including metamaterial cloaks designed based on transformation optics (TO) theory,[1] perfect absorbers realized with Salisbury's approach[2] or impedance-matched metamaterials,[3,4] and mantle cloaks achieved based on scattering cancellation mechanism.[5,6] These approaches have their own advantages and drawbacks. For example, while ideal TO-based cloaks can in principle exhibit perfect cloaking performances, they are difficult to realize in practice due to extreme material parameters required. Absorbers can transform incident electromagnetic (EM) energy into heat, but their working bandwidths are typically narrow, and the inevitable thermal radiations from the object increase their possibilities of being detected at infrared frequencies. Mantle cloaks strongly rely on the shapes of the objects being cloaked, and suffer from a similar issue of narrow bandwidth.

Metasurfaces, planar metamaterials composed by subwavelength-sized meta-atoms with tailored EM properties, were recently proposed as an alternative approach to reduce radar cross sections (RCS).[7−25] The advantages of such a scheme are that a metasurface can be much thinner than wavelength and can easily accommodate with a curved surface of an arbitrary object being hidden. The principle mechanism of early attempts is to utilize the destructive interferences of fields scattered from different meta-atoms on the metasurface to reduce the total specular reflection. For example, two types of meta-atoms exhibiting an 180° reflection-phase difference were arranged in a chessboard configuration to form several RCS-reduction metasurfaces.[7−11] However, such a scheme suffers from the

Special Issue: Ultra-Capacity Metasurfaces with Low Dimension and High Efficiency

Received: September 11, 2017
Published: October 27, 2017

DOI: 10.1021/acsphotonics.7b01036
ACS Photonics 2018, 5, 1691−1702

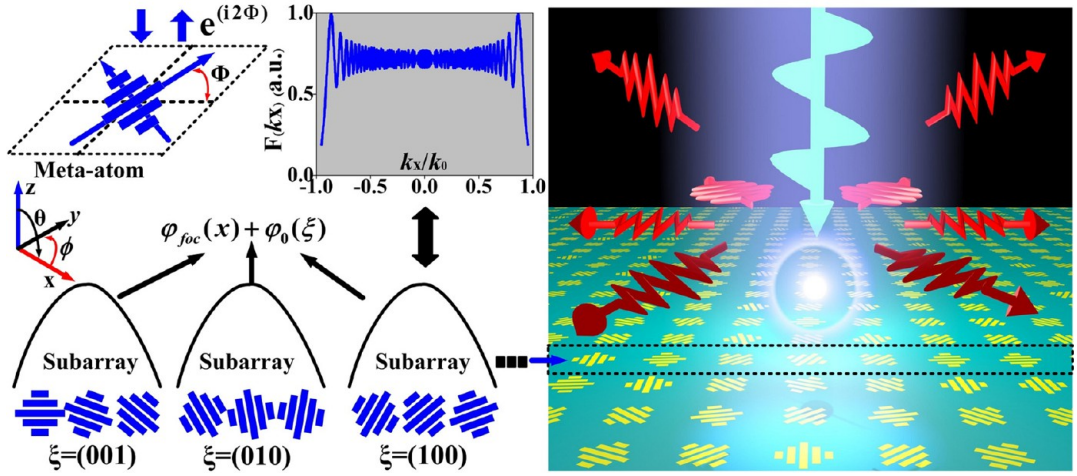

Figure 1. Conceptual illustration of the design processes and the wave-diffusion realized by our metasurface. Left panel describes the three key steps to design our metasurface consisting of spatially rotated meta-atoms: first design a reflective PB meta-atom with nearly 100% efficiency, and next use it to form a set of subarrays based on focusing phase profiles but with different initial phases by rotating PB meta-atoms with respect to z axis, and finally arrange these subarrays based on certain coding sequence. Inset shows a typical Fourier-transform spectrum of a focusing-phase subarray. Right panel illustrates the wave-diffusion behaviors achieved by our metasurface.

issues of narrow-bandwidth,[7] significantly degraded performances at off-normal incidences, and strong diffractions to certain angles.[8−11] To address these issues, metasurfaces with more different types of meta-atoms (exhibiting different reflection phases) arranged in more complex manners (e.g., gradient, coding, or even random sequences) were proposed, which can significantly broaden the working bandwidth[12] and enhance the RCS-reduction performances by redistributing the scattered energies to more different channels.[13−20] We note that attempts have also been made to improve the polarization and angle insensitivity of the scheme using miniaturized aperiodic meta-atoms[9,21] and to address the conflictions between stealth and signal emissions/detections.[22−24] Recently, continuously shaped metasurfaces were proposed to eliminate the phase noises induced by the phase discontinuities, yielding a better control over the scattered fields.[25]

Despite the fruitful progresses already achieved toward RCS reduction based on metasurfaces, several unaddressed issues hinder the practical applications of such a scheme. First of all, while most designed metasurfaces can indeed reduce the backward RCS significantly, their scatterings to some particular angles are not necessarily as low as the backward one, which may still enable the target visible under the bistatic detection. As a result, in order to achieve the best wave-diffusion performance (with nearly uniform low-intensity angular distributions), the coding sequences on which the meta-atoms are arranged should be carefully optimized (if existing), which are time-consuming and difficult to reproduce by different groups. Also, many RCS-reduction metasurfaces designed so far can only work for one particular linear-polarization excitation (although polarization controlled multi-functional devices for other applications have been extensively reported[26−28]), while in reality the incident EM wave can take any polarization. In this article, we propose a robust and deterministic approach to design metasurfaces that can diffusively scatter EM waves with arbitrary polarizations, within an ultrawide frequency band and for a wide-range incidence angles. The key idea in our approach is to adopt a focusing phase distribution to arrange our meta-atoms (widely used in meta-lens applications[29,30]), which can ensure a nearly uniform low-scatterings to all directions. The powerfulness of our approach is demonstrated by our experimental and simulation results, exhibiting much better wave-diffusion performances than other available approaches. Our results are important for fast designs of high-performance diffusive-scattering metasurfaces, which are crucial in stealth-related applications.

RESULTS

Design strategy. Our design strategy consists of three steps, as schematically depicted in Figure 1. We first design a totally reflective Pancharatnam−Berry (PB) meta-atom exhibiting wide-band high-efficiency cross-polarization conversion, then use it to construct a set of subarrays exhibiting the same focusing phase distributions for circularly polarized (CP) light but with different initial phases, and finally arrange these subarrays in an arbitrary coding order to form a metasurface. In what follows, we briefly argue why a metasurface designed in such a way can diffusively scatter incident EM waves.

The key motivation of using a PB meta-atom as the building block is to release the polarization sensitivity of the measurface's functionality. This is highly desired for the stealth and antistealth applications, where the polarization of impinging wave is typically unknown. Since any linearly polarized (LP) wave can be decoupled as a linear combination of two different CP waves, in what follows we focus on studying how to diffusively scatter CP waves. As discussed in refs 31−36, a PB meta-atom satisfying certain criterion can scatter incident CP wave with a PB phase factor $\exp(i\sigma 2\Phi)$, where $\sigma = 1$ denotes the left CP (LCP) light, while $\sigma = -1$ the right CP (RCP) light and Φ is the orientation angle of the meta-atom (see left panel in Figure 1).

With such a PB meta-atom designed, our next step is to determine how to arrange these meta-atoms, that is, the distribution of their orientation angle $\Phi(\vec{r}_{\parallel})$ or equivalently the distribution of reflection-phase for a particular CP light $\varphi(\vec{r}_{\parallel}) = 2\Phi(\vec{r}_{\parallel})$. Here, $\vec{r}_{\parallel} = (x,y)$ denotes a position on the meta-surface. According to Fermat-Huygens' law, wave scattered by a metasurface under normal excitation can be computed by summing up all contributions from different local positions at

DOI: 10.1021/acsphotonics.7b01036
ACS Photonics 2018, 5, 1691−1702

the metasurface. Thus, at a far-field point $\vec{R} = R\hat{n}$, EM field components are proportional to $G(\vec{R}) = \frac{1}{4\pi R}\int e^{i\varphi(x,y)} e^{ik\hat{n}\cdot(\vec{R}-\vec{r}_{\parallel})}\mathrm{d}x\mathrm{d}y$ where the integration runs over the whole metasurface and $k = \omega/c$ with ω and c being the frequency and the speed of light. Simple calculation indicates that the far-field scattering pattern of a meta-surface is closely related to the Fourier transform of its reflection-coefficient distribution $r(x, y) = e^{i\varphi(x, y)}$,

$$F(\vec{k}_{\parallel}) = \frac{1}{L^2}\int e^{i\varphi(x,y)} \mathrm{e}^{-i\vec{k}_{\parallel}\cdot\vec{r}_{\parallel}}\mathrm{d}x\mathrm{d}y \tag{1}$$

with L^2 being the total area of the meta-surface. Therefore, to achieve the best wave-diffusion performance, we need to select such a $\varphi(x, y)$ distribution that can make the $\vec{k}_{\parallel}$ dependence of the F function as uniform as possible.

While getting a rigorous solution of $\varphi(x, y)$ is difficult since it needs solving an inverse problem, we can gain physical insights by examining some well-studied cases. To simplify our discussions, we consider the one-dimensional (1D) case where the reflection-phase only varies against x. Obviously, a uniform or a linearly varying phase profile $\varphi(x, y) = \text{const.} + \xi_0 \cdot x$ does not fulfill our requirement, since there Fourier transforms are delta-like functions $\sin c\left(\frac{1}{2}(\xi_0 - k_x)L\right)$, indicating that the meta-surface will scatter incident waves to some specific directions. Meanwhile, we find that the focusing phase profile, $\varphi_{\mathrm{foc}}(x, y) = \frac{2\pi}{\lambda}(\sqrt{x^2 + y^2 + f^2} - f)$ with f being the focal length and λ the working wavelength, adopted frequently in meta-lensing applications,[29,30] can exhibit a much smoother $F \sim k_x$ relation, as shown in the inset to Figure 1. This is quite understandable, since a meta-lens can focus an incident plane wave to a point (line), and thus, the wave re-emitted from a single point (line) must exhibit a very uniform angular distribution.

Such an attractive Fourier-transform property motivates us to use the focusing phase profile to arrange our PB meta-atoms. However, directly applying a single focusing phase profile to design a realistic sample may encounter the following issues. First, in practical applications, the input beam may not be a plane wave and usually exhibits a finite beam size with a beam center. In the latter case, the wave-diffusion effects will be significantly degraded when the beam-center is not right at the original point of the metasurface. Second, a realistic wave-diffusion screen may not always exhibit a circular shape but rather exhibit an arbitrary shape and size, in order to fit the request of practical applications. Therefore, the focusing phase profile may become significantly distorted at the boundaries of a metasurface with arbitrary shape and size, thus yielding undesired strong scatterings. To solve above issues, we introduce the final design step borrowing the concept of coding metasurface, which is now widely used in controlling both EM waves[15,37] and acoustic waves.[38,39] Instead of arranging the PB meta-atoms based on a single global focusing phase profile, here we cut a large metasurface into small square-shaped pieces called "subarrays". Inside each subarray consisting of $P \times P$ meta-atoms, we arrange the orientations of PB meta-atoms according to the following local focusing phase profile for LCP light:

$$\begin{aligned}\varphi(u, v) &= \varphi_{\mathrm{foc}}(u, v) + \varphi_0(\xi) \\ &= \frac{2\pi}{\lambda}(\sqrt{u^2 + v^2 + f^2} - f) + \varphi_0\end{aligned} \tag{2}$$

where (u, v) denotes the center position of a meta-atom in the local coordinate system of a subarray. In addition to a conventional focusing profile denoted as $\varphi_{\mathrm{foc}}(u, v)$, we purposely add an initial phase φ_0 to the expression (see eq 2). While this term does not affect the Fourier transform spectrum and is thus usually neglected in conventional meta-lens applications, here we find that it can serve as an important parameter to distinguish different subarrays. We can thus use this parameter to construct a series of "bits" borrowing the idea from coding metasurfaces.[15,37] Specifically, a σ-bit metasurface ($\sigma = 1, 2, 3, \ldots$) contains 2^σ different types of subarrays, with the initial phase of the ξ^{th} subarray taking the value $\varphi_0(\xi) = 2\pi\xi/2^\sigma$. For example, in 1-bit realizations, we select two initial phases, $\varphi_0 = 0°, 180°$, to define two different type of subarrays labeled as the "(0)" and "(1)" states, while in 2-bit cases, we select four initial phases $\varphi_0 = 0°, 90°, 180°, 270°$ to define four states labeled as "(00)", "(01)", "(10)", and "(11)", respectively. The final step of designing our metasurface is to arrange these "bits" in an arbitrarily generated coding sequence. Figure 2a shows

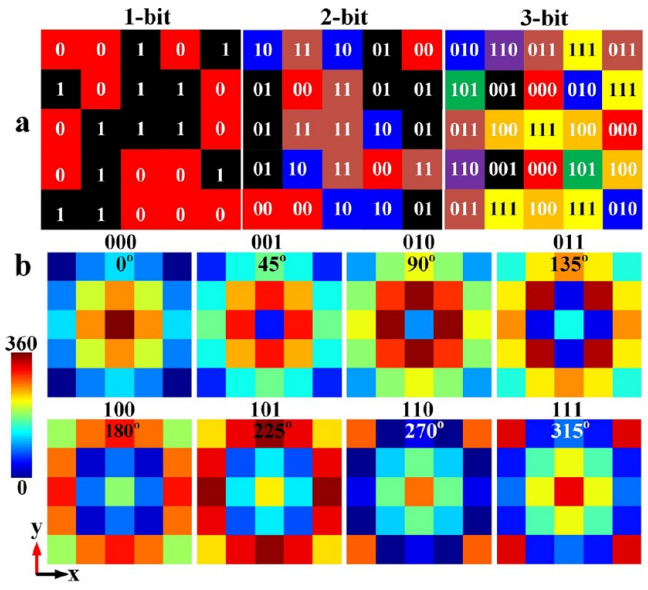

Figure 2. Design of the multibit focusing-phase coding metasurfaces. (a) Arbitrarily generated coding sequences for the 1-bit, 2-bit, and 3-bit metasurfaces studied in this paper. (b) Explicit phase distributions of eight different types of subarrays adopted in the 3-bit realizations. Here, each metasurface contains 5 × 5 subarrays and each subarray contains 5 × 5 meta-atoms, and the phase distributions are LCP incident light. Here, the focal length is chosen as f = 5 mm and the length of a square-shape meta-atom is a = 12 mm.

three arbitrarily generated coding sequences in 1-bit, 2-bit, and 3-bit realizations, respectively, and Figure 2b depicts the detailed meta-atom arrangements inside 8 different types of subarrays in the 3-bit systems. Full 360° phase coverage is clearly observed in each subarray. Such full 360° phase coverage is a criterion to determine the size of our subarray, which is crucial to achieve an ideal wave-diffusion effect with nearly uniform low scatterings to all directions (see Figures S2 and S4 in Supporting Information). We note that the "bits" adopted in 1-bit and 2-bit systems can be accordingly found in Figure 2b.

DOI: 10.1021/acsphotonics.7b01036
ACS Photonics 2018, 5, 1691−1702

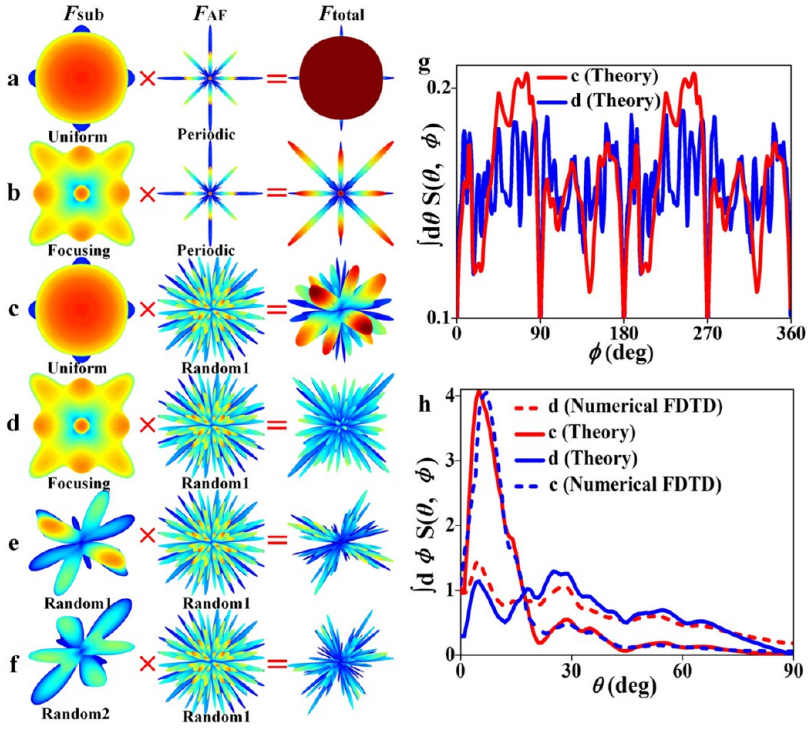

Figure 3. Scattering properties of metasurfaces with different subarrays and coding sequences analyzed by the array theory. Scattering patterns of metasurfaces constructed with subarrays exhibiting (a, c) uniform distribution, (b, d) focusing-phase distribution, and (e, f) random distribution, arranged in (a, b) a periodical lattice, (c–f) 1-bit coding sequence, as shown in Figure 2a (defined as random 1). Two different random distributions are adopted to arrange the intrasubarray meta-atoms in (e) and (f): while the distribution is just random 1 sequence in (e), it is random 2 sequence [1, 1, 1, 0, 0; 0, 0, 1, 1, 0; 1, 0, 1, 1, 1; 0, 1, 1, 0, 0; 1, 0, 0, 1, 0] in (f). The spectra of integrated scattering (g) $\int_0^{90^0} S(\theta, \phi)\mathrm{d}\theta$ and (h) $\int_0^{360^0} S(\theta, \phi)\mathrm{d}\phi$ at 14.6 GHz, obtained for different metasurfaces using the array theory and FDTD simulations on realistic structures.

For example, the "(01)" subarray in the 2-bit system is just the "(010)" subarray in the 3-bit system since they have exactly the same initial phase.

Now the advantages of our design strategy are clear. First, for any arbitrary-shaped screen, one can always "cut" it into small subarrays to accommodate a (local) focusing phase profile. Second, the wave-diffusion performance of a metasurface designed in such a way is insensitive to the center of incident beam. Third, cutting a large sample into subarrays with small size and regular shape can significantly reduce the corner scatterings on a large sample. All these attractive features make our design strategy robust and useful for practical applications. Finally, we emphasize that, although we borrowed the "coding" concept from the coding metasurfaces, the final wave-diffusion effect is quite robust against the concrete coding sequence being selected. In fact, the "coding" concept is introduced mainly to solve the finite-size and shape issues in realistic applications, and any moderate random sequence can be used to generate satisfactory wave-diffusion effect, as we demonstrate later. Such a feature distinguishes our work from previous efforts relying critically on the randomness provided by the coding sequence.[14−20]

Model Analyses. Before performing any realistic designs, we first employ the array theory (see Supporting Information) to justify the proposed design approach. Since here we consider a totally reflective system, the reflection amplitude of each meta-atom is 100%. For simplification, here we assume that our meta-atom has a size of $a \times a$ and the metasurface contains $L \times L$ subarrays. Extensions to more complicated cases are straightforward. We have used the array theory to derive the analytical formulas to compute the scattering patterns of metasurfaces described by eq 2 (see Supporting Information). We find that the contributions from the term $\varphi_{\mathrm{foc}}(u, v)$ (existing in all subarrays) can be factored out as a term solely dictated by the subarray, while the contributions from the initial phase $\varphi_0(\xi)$ yield another term which depends solely on the global coding sequence. Specifically, the scattered patterns of our designed metasurfaces, seen at a direction (θ, ϕ), can be theoretically computed as

$$s_{\mathrm{total}}(\theta, \phi) = \cos^2\theta \times |F_{\mathrm{sub}}(\theta, \phi)|^2 \times |F_{\mathrm{AF}}(\theta, \phi)|^2 \tag{3}$$

where

$$F_{\mathrm{sub}} = \sum_{m=0}^{P-1}\sum_{n=0}^{P-1} e^{i\cdot k\cdot ma\cdot \sin\theta\cos\phi} e^{i\cdot k\cdot na\cdot \sin\theta\sin\phi} e^{i\cdot\varphi_{\mathrm{foc}}(ma,na)} \tag{4a}$$

denotes the contribution from a single subarray,

$$F_{\mathrm{AF}} = \sum_{M=0}^{L-1}\sum_{N=0}^{L-1} e^{i\cdot k\cdot MPa\cdot \sin\theta\cos\phi} e^{i\cdot k\cdot NPa\cdot \sin\theta\sin\phi} e^{i\cdot\varphi_0(M,N)} \tag{4b}$$

accounts for the contribution from the global coding sequence, and the term $\cos^2\theta$ is contributed by a single PB meta-atom. Here, P^2 denotes the number of meta-atoms in each subarray. Note that the initial phase φ_0 of the subarray centered at the position (Ma, Na) is determined by its coding sequence (see Figure 2a). The powerfulness of this approach can be seen from

DOI: 10.1021/acsphotonics.7b01036
ACS Photonics 2018, 5, 1691−1702

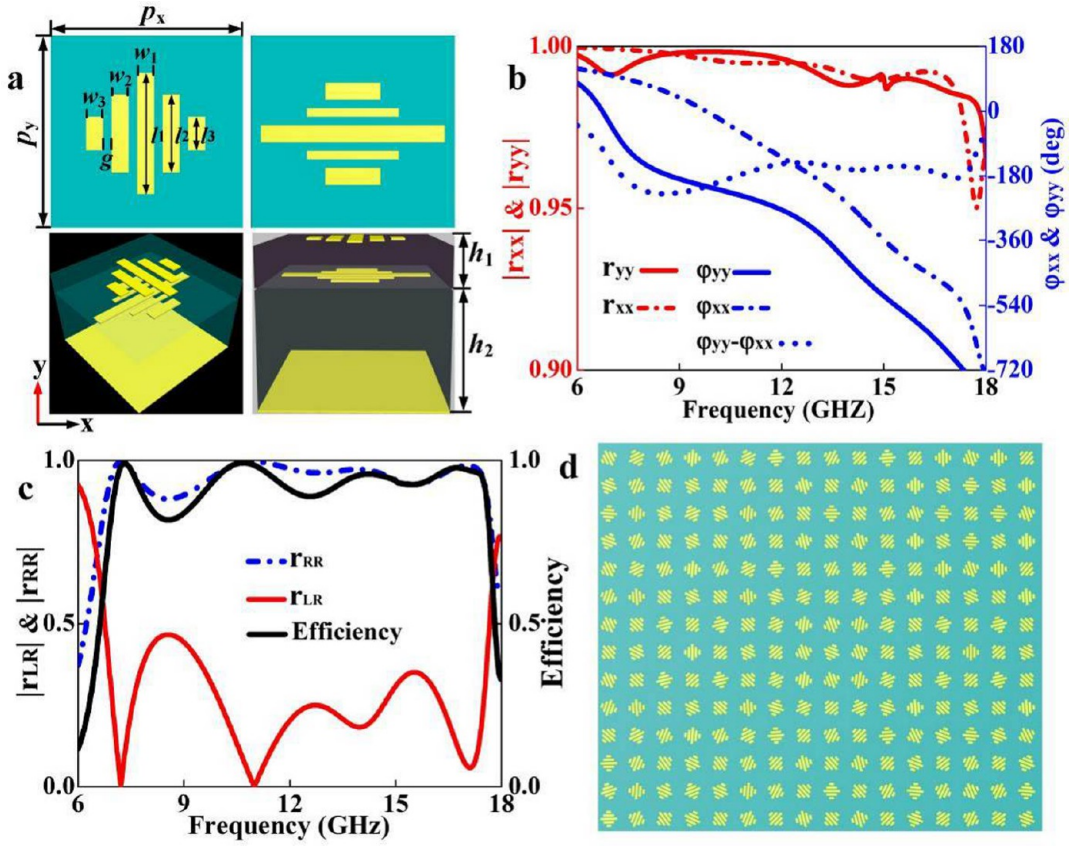

Figure 4. Design of the high-efficiency broadband PB meta-atom. (a) Layout of the designed meta-atom. FDTD calculated spectra of reflection coefficients of the meta-atom (periodically repeated to form an infinite plane) shined by (b) LP and (c) CP plane wave excitations. (d) Zoom-in-view of the explicit structure of the 3-bit metasurface designed in Figure 2. Here, the structure parameters are $l_1 = 7.11$, $l_2 = 4.59$, $l_3 = 1.98$, $w_1 = w_2 = w_3 = 1$, $g = 0.5$ (upper metallic pattern), $l_1 = 10.8$, $l_2 = 5.4$, $l_3 = 3.24$, $w_1 = w_3 = 1$, $w_2 = g = 0.5$ (lower metallic pattern), and $p_x = p_y = 12$, $h_1 = 0.3$, $h_2 = 3$, all of which have the units of mm. The subscripts "L" and "R" in (c) denote the LCP and RCP wave, respectively, and the working efficiency (black solid line) is calculated by the reflection coefficients according to eq 5.

the nice agreement between the calculations based on eq 3 and FDTD simulations (see Figure 3).

Figure 3 compares the performances of metasurfaces made with different subarrays and coding sequences. As expected, a metasurface composed by focusing-phase subarrays can always scatter EM wave to a mass of directions no matter its arrays are periodically repeated (Figure 3b) or in coding manner (Figure 3d). However, if a metasurface is composed by uniform-phase subarrays, it can enable partial wave diffusions toward several specific angles only when its arrays are arranged in a coding manner (Figure 3c), but behaves like an ordinary mirror when its arrays are arranged periodically (Figure 3a). We should emphasize that, a random-phase metasurface with all meta-atoms arranged randomly is not guaranteed to exhibit satisfactory wave diffusions if its randomness (i.e., the coding sequence) is not carefully optimized (see Figure 3e,f for two examples with arbitrarily generated sequences). Therefore, based on uniform- or random-phase subarrays, a coding metasurface can work for full wave-diffusion applications only after its coding sequence is carefully determined, which is not reproducible and needs sophisticated searching process. In contrast, based on our proposed scheme, one can easily achieve robust wave-diffusion properties based on an arbitrarily selected nonuniform coding sequence.

We select two planes to quantitatively compare the scattering performances of different metasurfaces. Figure 3g depicts how the integrated scattering powers over the angle ϕ vary against another parameter θ for different systems, while Figure 3h depicts similar curves but with ϕ and θ interchanged. As clearly shown, our proposed metasurface generates significantly more beams (peaks) in the ϕ plane than metasurfaces based on uniform-phase subarrays (see Figure 3g). Moreover, the energy scattered by our focusing-phase metasurface is greatly homogenized in the θ-plane, whereas a sharp beam is clearly observed for the uniform-phase coding metasurfaces.

Finally, we note that the scattering pattern of our focusing-phase subarray still exhibits some undesired peaks at certain azimuth angles (see Figure 3b,d), due to the square shape of the subarray. A circular-shape subarray works much better (see Figures S4 and S5 in Supporting Information), but is unfortunately not compatible to the metasurface design. Meanwhile, we re-emphasize that the numerical aperture (NA) of the lens (subarray) should be carefully selected. While a lens with a larger NA may provide more k-space distribution, it may suffer from off-normal aberrations or more severe aberrations at the boundary of the sub arrays. Considering all such competing facts, we note that a good criterion to determine the size of a subarray is that it should ensure full 360° reflection-phase coverage.

Design of the PB Meta-Atom. As the first step, we now design our realistic PB meta-atom. According to the theory presented in ref 36, the working efficiency of a PB metasurface strongly depend on the Jones's matric elements of the

DOI: 10.1021/acsphotonics.7b01036
ACS Photonics 2018, 5, 1691−1702

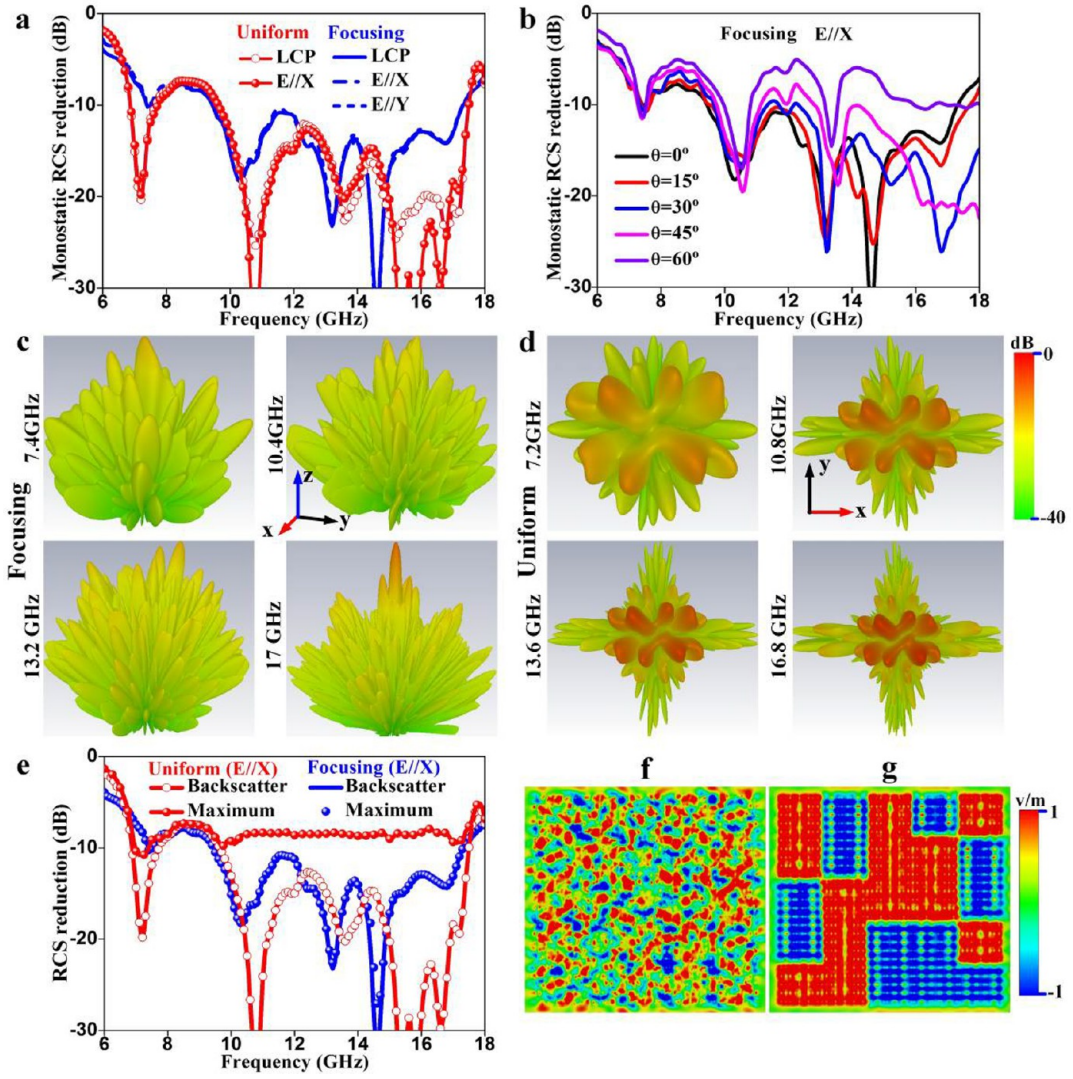

Figure 5. Numerical studies on the 1-bit metasurface. (a) FDTD calculated monostatic RCS reduction spectra of the metasurfaces with focusing-phase subarrays or uniform-phase subarrays arranged in the 1-bit coding manner, shined by incident plane waves with different polarizations. (b) FDTD calculated monostatic RCS reduction spectra of the 1-bit metasurface with focusing-phase subarrays shined by LP waves at different incident angles. (c, d) FDTD calculated 3D scattering patterns of the 1-bit metasurface using (c) focusing-phase subarrays or (d) uniform-phase subarrays. (e) Calculated spectra of maximum and backward-scattering RCS reduction for two metasurfaces under normal-incidence excitations. (f, g) Calculated near-field distributions of Re(E_x) at 13.2 GHz at the z = 5 mm plane above the two metasurfaces shined by x-polarized EM wave.

constitutional PB meta-atom. In particular, in present reflection geometry, the working efficiency can be expressed as

$$\eta = 2|(r_{xx} - r_{yy})/2|^2/[|r_{xx}|^2 + |r_{xy}|^2 + |r_{yx}|^2 + |r_{yy}|^2] \quad (5)$$

where r_{xx} and r_{yy} are the reflection coefficients of the meta-atom. Recalling that $|r_{xx}| = |r_{yy}| = 1$ in present cases (without considering the losses), we immediately understand that the highest working efficiency can be achieved when the condition $\varphi_{xx} - \varphi_{yy} = 180°$ is satisfied.

Based on this criterion, we propose a reflective multi-resonance meta-atom with geometry shown in Figure 4a. The meta-atom consists of two layers of metallic planar resonators and a metallic ground plane, and two F4B dielectric spacers ($\varepsilon_r = 2.65 + 0.001i$) to separate these metallic layers. Each metallic structure consists of five metallic bars with geometrical parameters carefully adjusted to tune the resonant frequencies.[33] Such a multilayer structure fully utilizes the vertical space to integrate multiple resonators with adjustable properties in a more compact way than its planar-arrangement counterpart.[40] Since the bar orientations in two metallic planes are orthogonal, the reflection responses for two incident polarizations can be engineered nearly independently, and therefore our meta-atom can easily realize the desired 180° phase-difference for two orthogonal polarizations as compared to the structure based on continuous phase modulation.[41] Although one can combine the metallic structures on two top layers to form a single metallic layer,[36] the physical connection between metallic bars must be avoided, which places unfavorable restrictions on the design. As a result, the performance (e.g., working efficiency and bandwidth) of the meta-atom designed in this way might not be as good as that achieved with the present multilayer meta-atom, due to lacking of design freedoms. With the help of the dispersion engineering method,[42] we adjusted all geometrical parameters in such way to appropriately cascade the generated resonant modes, so that the condition ($\varphi_{xx} - \varphi_{yy} = 180°$) can be fulfilled within a frequency band as wide as possible.

DOI: 10.1021/acsphotonics.7b01036
ACS Photonics 2018, 5, 1691−1702

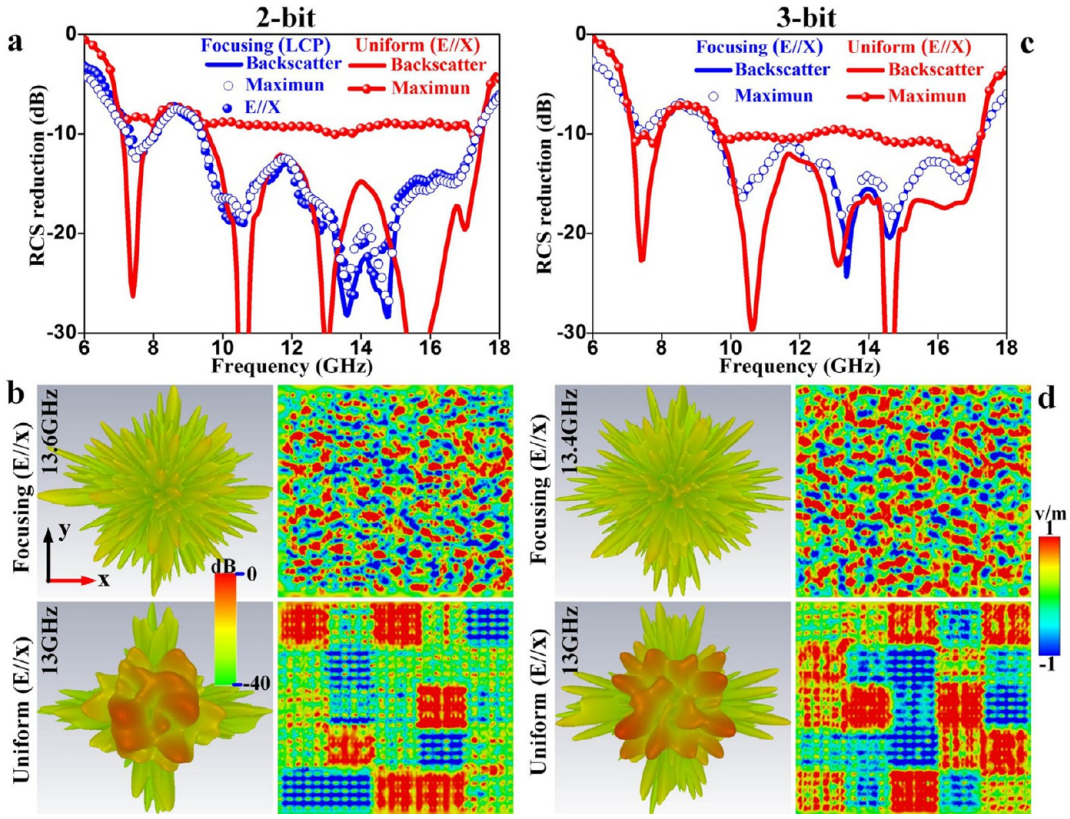

Figure 6. Numerical comparisons of scattering properties of the 2-bit and 3-bit metasurfaces. (a, c) FDTD calculated maximum and monostatic RCS reduction spectra of the (a) 2-bit and (c) 3-bit metasurfaces with focusing-phase and uniform-phase subarrays shined by normal-incidence waves with different polarizations. (b, d) Calculated 3D scattering patterns (left panel) and near-field distributions of Re(E_x) at z = 5 mm (right panel) under x-polarized EM wave of the (b) 2-bit and (d) 3-bit metasurfaces.

The FDTD computed Jones' matrix characteristics of the optimized PB meta-atom (periodically replicated to form an infinite plate) are depicted in Figure 4b. Within a wide frequency band 6.95−17.6 GHz, we do find that $|r_{xx}| = |r_{yy}| \approx 1$ (with realistic losses considered) and the condition $\varphi_{xx} - \varphi_{yy} = 180°$ is approximately satisfied. To quantitatively see the performance of our designed meta-atom, we employed eq 5 to compute the working efficiency of the PB meta-atom and then depicted in Figure 4c how the efficiency varies against frequency. As shown in Figure 4c, the working efficiency of our designed PB meta-atom remains higher than 0.8 within 6.9−17.6 GHz, in which the copolarization reflection is dominant ($|r_{RR}| > 0.89$) with desired polarization extinction ratio $\sigma = 20 \log_{10}(|r_{RR}|/|r_{LR}|) > 5.6$ dB under CP excitations. Such an attractive feature makes our PB meta-atom working in an ultrawide frequency band suffering nearly no frequency dispersions, being very important for practical applications.

With such a wide-band high-efficiency PB meta-atom designed, we then use it as a building block to design the RCS-reduction metasurfaces according to the strategy described in last section. In this paper, without losing generality, we study three metasurfaces with phase distributions explicitly presented in Figure 2 (see also Figure S8 in Supporting Information). Figure 4d depicts part of the layout for the 3-bit metasurface, and detailed layouts of the 1-bit, 2-bit, and 3-bit metasurfaces can be seen in Figure S9 in Supporting Information. In the next sections, we will first employ numerical simulations to analyze the RCS reduction performances of these metasurfaces and then experimentally verify the predictions based on realistic samples fabricated.

Numerical Studies on the Designed Metasurfaces. We first numerically study the scattering properties of the 1-bit metasurface. Figure 5a plots the FDTD calculated spectra of monostatic RCS reduction (e.g., the backward scattering) of our 1-bit focusing-phase metasurface (blue lines), under the illumination of incident waves with different polarizations. First, we note that the final results are independent of the incident polarization, which is one key advantage of employing a PB meta-atom as the building block, also noted in other recent works.[17] More importantly, the backward scattering of our metasurface has been significantly reduced in the entire frequency band considered, with the −7.5 dB RCS reduction bandwidth 11 GHz (from 7 to 18 GHz) yielding a fractional bandwidth 88%. Such a broadband backward RCS reduction even holds at oblique incidence for angles up to 60°, as shown in Figure 5b. We note that several reflection peaks and dips exist in the monostatic RCS reduction spectra (Figure 5a), which are caused by the variations of the $\varphi_{xx} - \varphi_{yy}$ spectrum of the PB meta-atom (Figure 4b). One important advantage of our metasurface is that it can diffusively scatter the incident waves to nearly all different channels, not just suppressing the backward scatterings. To demonstrate this point, we show in Figure 5c the computed three-dimensional (3D) radiation patterns of our 1-bit focusing-phase metasurface, under normal incident excitations at four representative frequencies. Our metasurface can redistribute the scattering waves uniformly toward countless angles in the whole upper half-space. Such an attractive scattering characteristic is also proved by Figure S10 in Supporting Information, where the scattering patterns are plotted in two principal planes.

DOI: 10.1021/acsphotonics.7b01036
ACS Photonics 2018, 5, 1691−1702

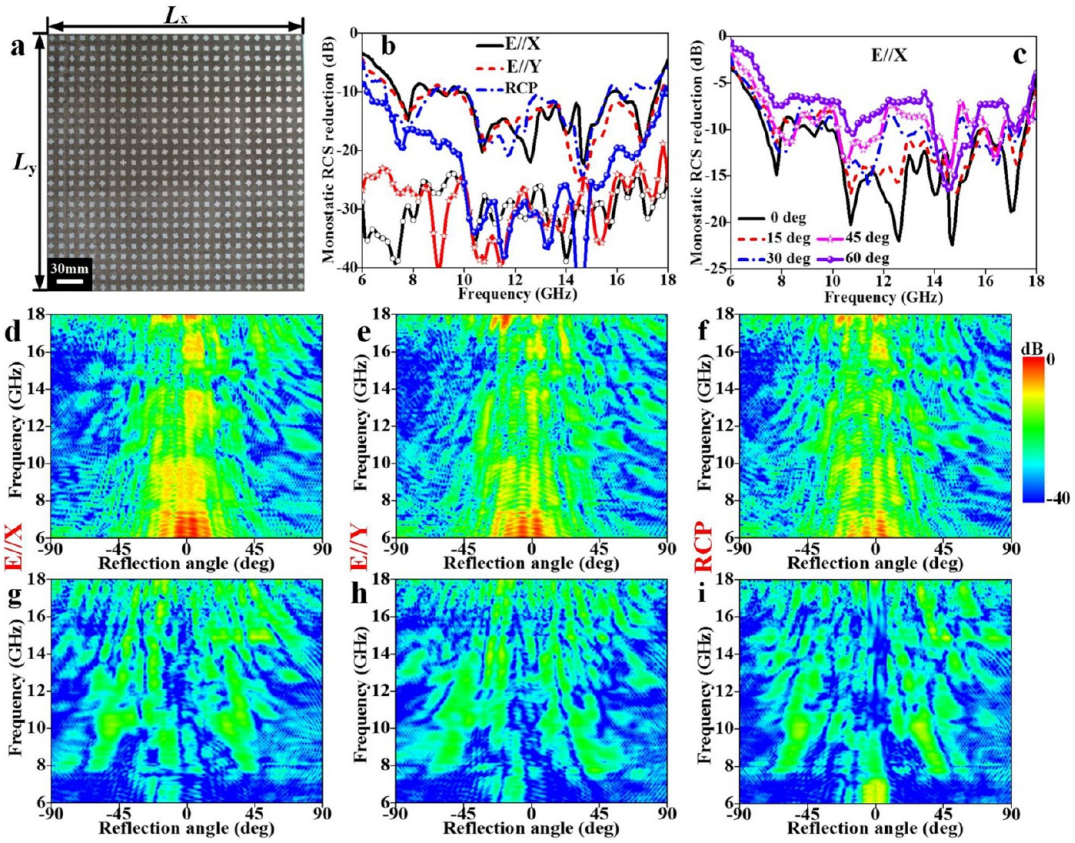

Figure 7. Experimental characterizations on the fabricated 1-bit metasurface. (a) Photograph of the fabricated sample. (b) Measured copolarized (lines) and cross-polarized (symbols) monostatic RCS reduction of the sample under normal-incidence excitations with different polarizations. (c) Measured copolarized monostatic RCS reduction of the sample shined by TE-polarized obliquely incident microwaves at different incident angles. Measured (d–f) copolarized and (g–i) cross-polarized RCS reduction in *H* plane as a function of frequency and reflection angles of the sample under normal-incidence excitations with different polarizations.

We compared the wave-diffusion properties of our 1-bit metasurface with a conventional 1-bit metasurface exhibiting identical coding sequence but with uniform-phase subarrays. While the latter can achieve good backward-scattering reductions (solid and dotted lines in Figure 5a) independent of the incident polarization (an intrinsic property of the PB meta-atom), the 3D patterns depicted in Figure 5d reveal that waves scattered by such a metasurface are only dispersed into several particular angles and thus low scattering intensity is observed only around the normal direction. As a result, if we compare the performances of two metasurfaces in terms of maximum scatterings in the whole angle region instead of only the backward ones, we find that our focusing-phase-based metasurface behaves much superior than the uniform-phase-based metasurface, as shown by the blue lines in Figure 5e. Such partial-diffusion property of the uniform-phase-based metasurface makes the hidden object still being possibly detected by the bistatic detection.

To understand the intrinsic physics why the two metasurfaces behave so differently, we depict in Figure 5f,g the near-field E_x distributions on two metasurfaces shined by *x*-polarized waves at 13.2 GHz. We note that the near-field distributions on two metasurfaces are completely different although they exhibit identical global coding sequence. While in uniform-phase coding metasurface we only find two types of pixels with 180° phase difference, a mass of field fragments with different phases are observed in the focusing-phase-based metasurface. The physics is thus clear: the purposely selected (local) focusing phase profile inside the subarrays enable the metasurface further disturb the phase coherences of different radiating sources (the PB meta-atoms) thus generating much improved diffusive-scattering performances.

As we mentioned in previous sections, the full wave-diffusion ability of our metasurface is quite independent of the coding sequence selected, and any sequence with moderate randomness can achieve satisfactory effects. We now use numerical simulations to demonstrate this point. Figure 6 contains our numerical studies on the scattering patterns of the 2-bit and 3-bit coding metasurfaces, which are constructed based on the same focusing-phase subarrays but arranged in different global coding sequences (see Figure S9 in Supporting Information for their explicit layouts). As shown in Figure 6a,c, the two metasurfaces, although in different coding sequences, both exhibit broadband low-scattering RCS spectra. The −7.5 dB backward RCS reduction bandwidths are found as 10.75 and 10.5 GHz for two metasurfaces, respectively. Very similar wave-diffusions with near-uniform intensity toward countless angles are again observed around 13 GHz (see top row in Figure 6b,d). More detailed information on the scattering properties of the two metasurfaces can be found in Figures S11 and S12 in Supporting Information. Moreover, the advantage of our method with respect to its random-phase counterpart can be seen from Figure S13 in Supporting Information.

In contrast, if the focusing-phase subarrays are replaced by uniform-phase ones, the scattering waves from the metasurfaces were again directed toward several specific angles, being

DOI: 10.1021/acsphotonics.7b01036
ACS Photonics 2018, 5, 1691–1702

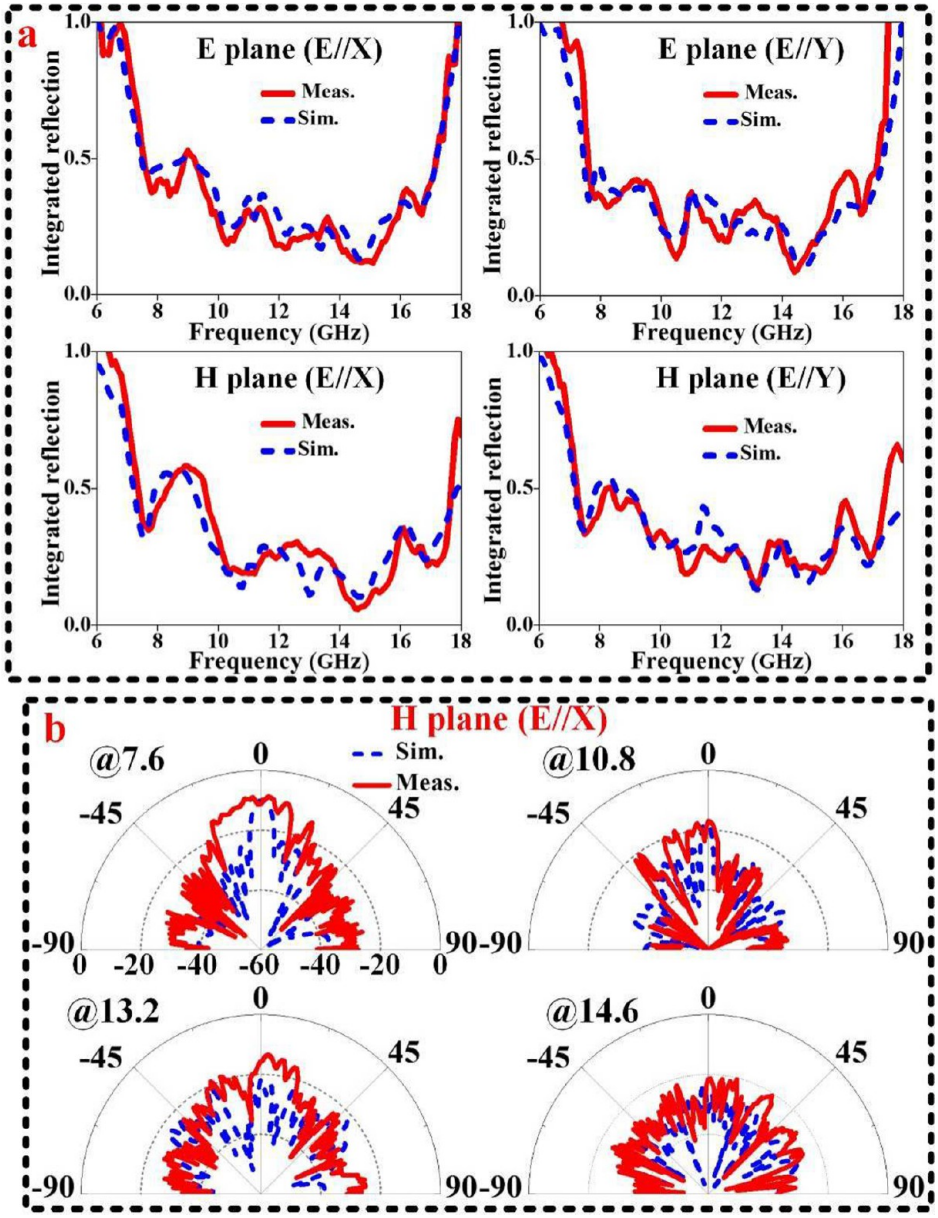

Figure 8. Comparisons between simulation and experimental results on the 1-bit metasurface. (a) Normalized integrated reflections ($\int S(\theta,\phi)\mathrm{d}\theta/\int S_0(\theta,\phi)\mathrm{d}\theta$, with $S(\theta,\phi)$ and $S_0(\theta,\phi)$ being angular spectra of scatterings of the metasurface and a metal plate of the same size) on E and H planes under normal-incidence excitations with different polarizations. (b) H-plane scattering patterns of the metasurface shined by normally incident x-polarized waves at four representative frequencies of 7.6, 10.8, 13.2, and 14.6 GHz, obtained by measurements and simulations.

unfavorable for realistic applications (see bottom row in Figure 6b,d). Specifically, we note that the maximum RCS reductions of such metasurfaces are around −9.3 and −9.7 dB, being much higher than those of our proposed metasurfaces constructed with focusing-phase subarrays (see Figure 6a,c). The underlying physics is again that the metasurfaces with focusing-phase subarrays can disturb the phases of the incident beam much more significantly that their uniform-phase counterparts, as shown in right column of Figure 6b,d.

We note that the specular-RCS and the 3D scattering patterns for three different metasurfaces (i.e., 1-bit, 2-bit, and 3-bit samples) are very similar, revealing that the wave-diffusion properties are very robust against the bit sequence. Such full-diffusion behaviors are only weakly dependent on the global coding sequence but are predominantly determined by the subarray structure exhibiting the focusing phase distribution. In contrast, the scattering patterns are very sensitive to the bit sequence for the coding metasurfaces constructed with subarrays with uniform phase distributions.

Experimental Results. We have performed microwave experiments to verify the wave-diffusion effects predicted in above sections. Without losing generality, we fabricated two realistic samples based on the 1-bit and 2-bit designs (see Figure S8 in Supporting Information for their layouts) using the standard printed-circuit-board (PCB) technology. Figures 7a and 9a depict the top-view photographs of the fabricated samples. We then characterized the scattering behaviors of these two metasurfaces in an anechoic chamber, with measurement details described in Methods.

We first measured the backward scattering spectrum of the 1-bit sample. As shown in Figure 7b, under normal incidence, the measured backward scattering of the 1-bit sample is 7 dB lower

DOI: 10.1021/acsphotonics.7b01036
ACS Photonics 2018, 5, 1691−1702

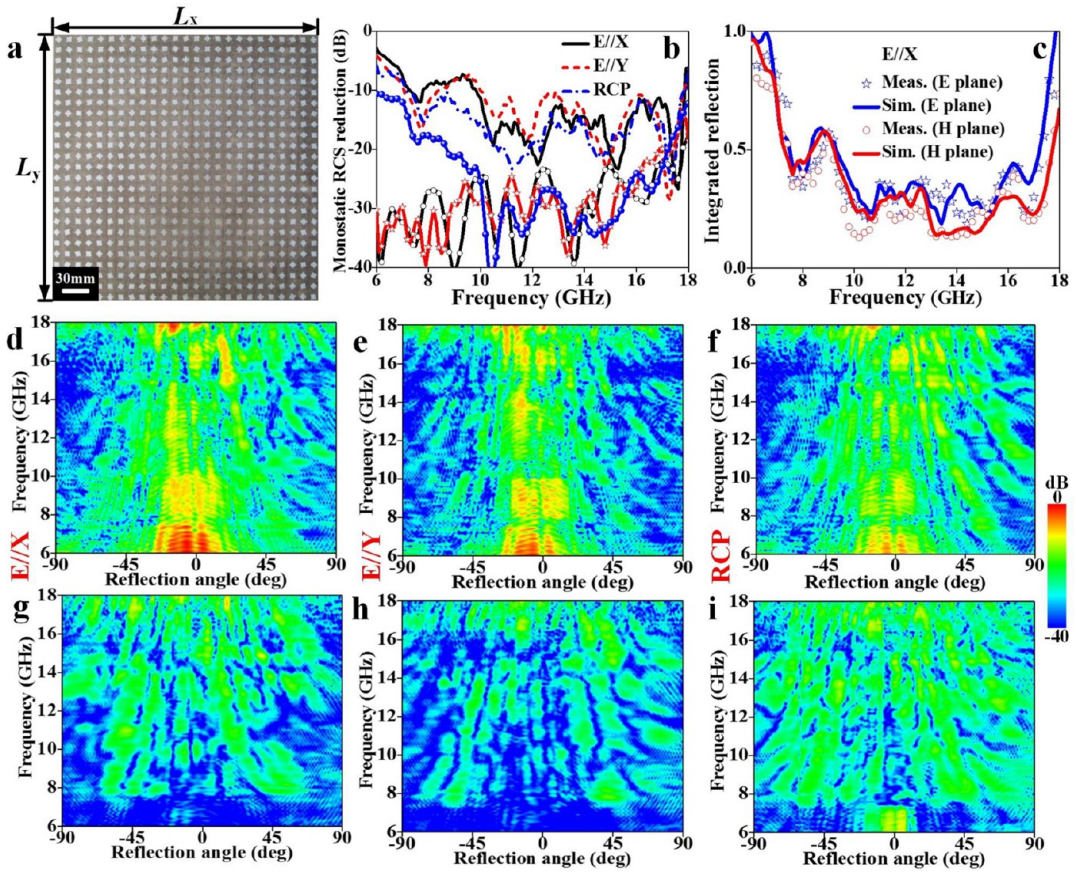

Figure 9. Experimental characterizations on the fabricated 2-bit metasurface. (a) Photograph of the fabricated sample. (b) Measured copolarized (lines) and cross-polarized (symbols) monostatic RCS reduction of the sample under normal-incidence excitations with different polarizations. (c) Comparison of simulated and measured normalized total reflections in *E* and *H* planes. Measured (d–f) copolarized and (g–i) cross-polarized RCS reduction in *H* plane as a function of frequency and reflection angle for the sample under normal incidence excitations with different polarizations.

than that of a metallic plate of the same size, within the frequency range (6.9–17.8 GHz) for all three incident polarizations. Several obvious reflection dips were found at 7.8, 10.8, and 14.6 GHz and the maximum RCS reduction reaches −25 dB, which coincide well with the FDTD calculated ones (Figure 5a). Considerable monostatic RCS reduction is also found for the 1-bit metasurface under oblique incidence, as shown in Figure 7c. The RCS reduction can be better than −5 dB within 7.3–17.8 GHz even when the incidence angle is up to 60°, confirming the wide-angle low-scattering behavior of our designed meta-surface.

We note that the cross-polarized and copolarized back-scattering are significantly different. This is because our PB meta-atom is designed as a (nearly perfect) reflection-mode half wave-plate satisfying the criterion $\varphi_{xx} - \varphi_{yy} = 180°$. Consider the case that the metasurface is shined by a CP wave with a particular handness. According to the theory presented in ref 36, the backscattered CP waves possessing the same handness as that of the incident one are the anomalous modes which can be manipulated by the PB metasurfaces, while the waves-components with handness reversed are the normal modes which can only be specularly reflected. With this in mind, one may easily prove that the behaviors of cross-polarized and copolarized backscattering are completely different when the metasurface is shined by a LP wave with an arbitrary polarization direction.

We next characterized the full angle spectra of the scattering patterns of the metasurface, in order to reveal its powerfulness to diffusively scatter EM waves. Figure 7d–i depicts the measured scattering power versus frequency and reflection angles in the *H* plane,[43] for the 1-bit metasurface shined by normally incident waves with three different polarizations. As expected, in all three cases studied, the scattered waves are redistributed toward innumerable directions for both copola-rization and cross-polarization reflections. We also performed the E-plane measurements for our sample and found very similar wave-diffusion behaviors (see Figure S14 in Supporting Information).

FDTD simulations (Figures 5 and S10 in Supporting Information) are in reasonable agreements with their corresponding experimental results. To quantitatively illustrate this point, we compared in Figure 8a the spectra of reflections integrated over the whole angle regions in *E* plane or *H* plane, obtained by FDTD simulations and experiments for the 1-bit sample under normal-incidence excitations with different polarizations. The measured and simulated spectra are all normalized against the corresponding reference values obtained based on a metal plate of the same size, under exactly the same conditions. In all cases studied, we found reasonable agreement between FDTD and experimental results, both showing low-scattering behaviors within a broad operation bandwidth. Figure 8b further compares the simulated and measured scattering patterns on different planes and at different frequencies. The obtained patterns exhibit clear diffusion characteristics, with wave scattered toward enormous angles

DOI: 10.1021/acsphotonics.7b01036
ACS Photonics 2018, 5, 1691–1702

with low intensities. The maximum scatterings are found lower than −12.1 dB, exhibiting satisfactory wave-diffusion properties.

Finally, we illustrate the coding-sequence independence of the wave-diffusion properties of our proposed metasurfaces, through experimentally characterizing the 2-bit sample (see Figure 9a for its picture) using the same approach. Figure 9b–i contain all measured results of the 2-bit sample. As shown in Figure 9b, a 7 dB backward reflection suppression is observed within the frequency window 6.9–17.9 GHz, for all three incident polarizations studied. Overall, the wave-diffusion features of the 2-bit sample are quite similar to those of the 1-bit sample, reinforcing our notion that they are the intrinsic properties of our metasurfaces, robust against varying the coding sequence. Measured *E*-plane patterns can be found in Figure S15 in Supporting Information.

DISCUSSION

In summary, combining the concepts of PB phases, metalenses, and coding metasurfaces, we proposed a deterministic and robust approach to design metasurfaces that can achieve polarization-independent diffusive scatterings of electromagnetic waves within an ultrawide frequency band and for a wide range of incident angle. The key idea in the design approach is the adoption of a focusing-phase subarray that can intrinsically yield nearly uniform low-scatterings to all directions. Compared to other design approaches, our approach is fast, deterministic, and the designed metasurface can redistribute the incident energy to more channels with more uniform distribution. Experimental characterizations on two metasurfaces designed based on the proposed approach show that the −7 dB RCS reduction bandwidths reach 11 GHz corresponding to a fractional bandwidth of 88%, and the diffusion behaviors can hold for oblique incidence at angles up to 60°. Our strategy may find important applications in stealth/clocking applications under bistatic detection. Extending our concept to the transmission geometry is feasible, based on recent fast developments on realizing transmissive meta-atoms with few-layer structures.[44,45]

METHODS

Simulations. In our FDTD simulations to calculate the reflection amplitudes/phases of the meta-atom, we studied a unit cell containing one meta-atom with periodic conditions imposed at the four boundaries of the unit cell, and then defined a Floquet port at a distance 15 mm away from the *xy*-plane where the meta-atom is placed. In the far-field and near-field calculations, we studied square-shape metasurfaces formed by 5 × 5 subarrays each consisting of 5 × 5 meta-atoms, with open boundary conditions set at its four boundaries. In all cases studied, the metasurface/meta-atom is shined by a normally incident *x*-, *y*-, LCP-, and RCP-polarized plane wave.

Microwave Experiments. All samples were characterized in a microwave anechoic chamber, using an angle-resolved experimental setup shown in Figure S16 of Supporting Information. In specular-reflection measurement, we adopted two double-ridged LP or CP horns as the emitter and receiver, placed 1 mm away from the sample with a 10° angle separation. The LP horns exhibit a voltage standing wave ratio (VSWR) less than 2.5 within the frequency range 1–18 GHz, whereas the two CP horns have VSWR ≤ 2.5 and axial ratio (AR) less than 3.5 dB within 6–18 GHz. These horns are connected to an Agilent N5230C vector network analyzer through two 13 m-long cables. In bistatic reflection measurements, the emitting horn and the metasurface were fixed on a big foam platform which can be rotated freely along its axial center. A receiving horn aligned with the metasurface is placed 1 m away from the rotated platform to record the signal scattered within the angle range $-90° < \theta_r < 90°$. In all cases studied, we used the specular-reflection signal received from a metal plate of the same size under the same excitation condition as the reference.

ASSOCIATED CONTENT

Supporting Information

The Supporting Information is available free of charge on the ACS Publications website at DOI: 10.1021/acsphotonics.7b01036.

Derivations of the array-theory formulas eqs 3 and 4; scattering properties of linear-phase metasurfaces; scattering properties of the focusing-phase subarrays and the criterion to determine the optimal size of a subarray; optimization of the focusing-phase metasurface; scattering properties of a quasi-periodic focusing-phase metasurface; additional FDTD results for focusing-phase metasurfaces; FDTD results for a random-phase metasurface; additional experimental results for the focusing-phase metasurfaces; pictures of the experimental setup (PDF).

AUTHOR INFORMATION

Corresponding Authors

*E-mail: phzhou@fudan.edu.cn.
*E-mail: hexiuxu@fudan.edu.cn.

ORCID

He-Xiu Xu: 0000-0003-0156-7642

Notes

The authors declare no competing financial interest.

ACKNOWLEDGMENTS

This work was supported by National Natural Science Foundation of China (Grant Nos. 11734007, 61501499, 11474057, 11674068, 11404063, and 11604167), National Key Research and Development Program of China (No. 2017YFA0303500), National Defense Foundation of China under Grant No. 2201078, Innovative Talents Cultivate Program of Shaanxi Province under Grant No. 2017KJXX-24, Shanghai Science and Technology Committee (Grant Nos. 16JC1403100 and 16ZR1445200), Natural Science Foundation of Shaanxi Province under Grant No. 2016JQ6001, and also Aviation Science Foundation of China under Grant No. 20161996009.

REFERENCES

(1) Liu, R.; Ji, C.; Mock, J. J.; Chin, J. Y.; Cui, T. J.; Smith, D. R. Broadband ground-plane cloak. *Science* **2009**, *323*, 366–369.
(2) Fante, R. L.; Mccormack, M. T. Reflection properties of Salisbury screen. *IEEE Trans. Antennas Propag.* **1988**, *36*, 1443–1454.
(3) Landy, N. I.; Sajuyigbe, S.; Mock, J. J.; Smith, D. R.; Padilla, W. J. Perfect metamaterial absorber. *Phys. Rev. Lett.* **2008**, *100*, 207402.
(4) Xu, H. X.; Wang, G. M.; Qi, M. Q.; Liang, J. G.; Gong, J. Q.; Xu, Z. M. Triple-band polarization-insensitive wide-angle ultra-miniature metamaterial transmission line absorber. *Phys. Rev. B: Condens. Matter Mater. Phys.* **2012**, *86*, 205104.
(5) Chen, P. Y.; Soric, J.; Alù, A. Invisibility and cloaking based on scattering cancellation. *Adv. Mater.* **2012**, *24*, OP281–OP304.

DOI: 10.1021/acsphotonics.7b01036
ACS Photonics 2018, 5, 1691–1702

(6) Liu, S.; Xu, H. X.; Zhang, H. C.; Cui, T. J. Tunable ultrathin mantle cloak via varactor-diode-loaded metasurface. *Opt. Express* **2014**, *22*, 13403−13417.
(7) Paquay, M.; Iriarte, J. C.; Ederra, I.; Gonzalo, R.; Maagt, P. D. Thin AMC Structure for Radar Cross-Section Reduction. *IEEE Trans. Antennas Propag.* **2007**, *55*, 3630−3638.
(8) Galarregui, J. C. I.; Pereda, A. T.; Falcón, J. L. M. D.; Ederra, I.; Gonzalo, R.; Maagt, P. D. Broadband radar cross-section reduction using AMC technology. *IEEE Trans. Antennas Propag.* **2013**, *61*, 6136−6143.
(9) Edalati, A.; Sarabandi, K. Wideband, wide angle polarization independent RCS reduction using nonabsorptive miniaturized-element frequency selective surfaces. *IEEE Trans. Antennas Propag.* **2014**, *62*, 747−754.
(10) Chen, W.; Balanis, C. A.; Birtcher, C. R. Checkerboard EBG surfaces for wideband radar cross section reduction. *IEEE Trans. Antennas Propag.* **2015**, *63*, 2636−2645.
(11) Pan, W.; Huang, C.; Pu, M.; Ma, X.; Cui, J.; Zhao, B.; Luo, X. Combining the absorptive and radiative loss in metasurfaces for multi-spectral shaping of the electromagnetic scattering. *Sci. Rep.* **2016**, *6*, 21462.
(12) Li, Y.; Zhang, J.; Qu, S.; Wang, J.; Chen, H.; Xu, Z.; Zhang, A. Wideband radar cross section reduction using two-dimensional phase gradient metasurfaces. *Appl. Phys. Lett.* **2014**, *104*, 221110.
(13) Ke, W.; Jie, Z.; Qiang, C.; Di, S. D.; Cui, T. J. Broadband and broad-angle low-scattering metasurface based on hybrid optimization algorithm. *Sci. Rep.* **2015**, *4*, 5935.
(14) Dong, D. S.; Yang, J.; Cheng, Q.; Zhao, J.; Gao, L. H.; Ma, S. J.; Liu, S.; Chen, H. B.; He, Q.; Liu, W. W. Terahertz broadband low-reflection metasurface by controlling phase distributions. *Adv. Opt. Mater.* **2015**, *3*, 1405−1410.
(15) Gao, L. H.; Cheng, Q.; Yang, J.; Ma, S. J.; Zhao, J.; Liu, S.; Chen, H. B.; He, Q.; Jiang, W. X.; Ma, H. F. Broadband diffusion of terahertz waves by multi-bit coding metasurfaces. *Light: Sci. Appl.* **2015**, *4*, e324.
(16) Zhao, Y.; Cao, X.; Gao, J.; Sun, Y.; Yang, H.; Liu, X.; Zhou, Y.; Han, T.; Chen, W. Broadband diffusion metasurface based on a single anisotropic element and optimized by the simulated annealing algorithm. *Sci. Rep.* **2016**, *6*, 23896.
(17) Chen, K.; Feng, Y.; Yang, Z.; Cui, L.; Zhao, J.; Zhu, B.; Jiang, T. Geometric phase coded metasurface: from polarization dependent directive electromagnetic wave scattering to diffusion-like scattering. *Sci. Rep.* **2016**, *6*, 35968.
(18) Su, P.; Zhao, Y.; Jia, S.; Shi, W.; Wang, H. An ultra-wideband and polarization-independent metasurface for RCS reduction. *Sci. Rep.* **2016**, *6*, 20387.
(19) Anders, P.; Fei, D.; Chen, Y.; Radko, I. P.; Bozhevolnyi, S. I. Random-phase metasurfaces at optical wavelengths. *Sci. Rep.* **2016**, *6*, 28448.
(20) Zhang, Y.; Liang, L.; Yang, J.; Feng, Y.; Zhu, B.; Zhao, J.; Jiang, T.; Jin, B.; Liu, W. Broadband diffuse terahertz wave scattering by flexible metasurface with randomized phase distribution. *Sci. Rep.* **2016**, *6*, 26875.
(21) Hou, Y. C.; Liao, W. J.; Tsai, C. C.; Chen, S. H. Planar multilayer structure for broadband broad-angle RCS reduction. *IEEE Trans. Antennas Propag.* **2016**, *64*, 1859−1867.
(22) Pan, W.; Huang, C.; Chen, P.; Ma, X.; Hu, C.; Luo, X. A low-RCS and high-gain partially reflecting surface antenna. *IEEE Trans. Antennas Propag.* **2014**, *62*, 945−949.
(23) Yang, P.; Yan, F.; Yang, F.; Dong, T. Microstrip phased-array in-band RCS reduction with a random element rotation technique. *IEEE Trans. Antennas Propag.* **2016**, *64*, 2513−2518.
(24) Liu, Y.; Li, K.; Jia, Y.; Hao, Y.; Gong, S.; Guo, Y. J. Wideband RCS reduction of a slot array antenna using polarization conversion metasurfaces. *IEEE Trans. Antennas Propag.* **2016**, *64*, 326−331.
(25) Guo, Y.; Yan, L.; Pan, W.; Shao, L. Scattering engineering in continuously shaped metasurface: An approach for electromagnetic illusion. *Sci. Rep.* **2016**, *6*, 30154.
(26) Chen, W. T.; Yang, K. Y.; Wang, C. M.; Huang, Y. W.; Sun, G.; Chiang, I. D.; Liao, C. Y.; Hsu, W. L.; Lin, H. T.; Sun, S. High-efficiency broadband meta-hologram with polarization-controlled dual images. *Nano Lett.* **2014**, *14*, 225−230.
(27) Xu, H. X.; Tang, S.; Ling, X.; Luo, W.; Zhou, L. Flexible control of highly-directive emissions based on bifunctional metasurfaces with low polarization cross-talking. *Ann. Phys.* **2017**, *529*, 1700045.
(28) Cai, T.; Tang, S. W.; Wang, G. M.; Xu, H. X.; Sun, S. L.; He, Q.; Zhou, L. High-performance bifunctional metasurfaces in transmission and reflection geometries. *Adv. Opt. Mater.* **2017**, *5*, 1600506.
(29) Xu, H. X.; Ma, S.; Luo, W.; Cai, T.; Sun, S.; He, Q.; Zhou, L. Aberration-free and functionality-switchable meta-lenses based on tunable metasurfaces. *Appl. Phys. Lett.* **2016**, *109*, 193506.
(30) Chen, X.; Huang, L.; Mühlenbernd, H.; Li, G.; Bai, B.; Tan, Q.; Jin, G.; Qiu, C. W.; Zhang, S.; Zentgraf, T. Dual-polarity plasmonic metalens for visible light. *Nat. Commun.* **2012**, *3*, 1198.
(31) Qin, F.; et al. Hybrid bilayer plasmonic metasurface efficiently manipulates visible light. *Sci. Adv.* **2016**, *2*, e1501168.
(32) Yin, X.; Zhang, X. Photonic spin hall effect at metasurfaces. *Science* **2013**, *339*, 1405−1407.
(33) Liu, Z.; Li, Z.; Liu, Z.; Li, J.; Cheng, H.; Yu, P.; Liu, W.; Tang, C.; Gu, C.; Li, J. High-performance broadband circularly polarized beam deflector by mirror effect of multinanorod metasurfaces. *Adv. Funct. Mater.* **2015**, *25*, 5428−5434.
(34) Phillion, R. H.; Okoniewski, M. Lenses for circular polarization using planar arrays of rotated passive elements. *IEEE Trans. Antennas Propag.* **2011**, *59*, 1217−1227.
(35) Florencio, R.; Encinar, J. A.; Boix, R. R.; Losada, V.; Toso, G. Reflectarray antennas for dual polarization and broadband telecom satellite applications. *IEEE Trans. Antennas Propag.* **2015**, *63*, 1234−1246.
(36) Luo, W.; Xiao, S.; He, Q.; Sun, S.; Zhou, L. Photonic spin hall effect with nearly 100% efficiency. *Adv. Opt. Mater.* **2015**, *3*, 1102−1108.
(37) Cui, T. J.; Qi, M. Q.; Wan, X.; Zhao, J.; Cheng, Q. Coding metamaterials, digital metamaterials and programmable metamaterials. *Light: Sci. Appl.* **2014**, *3*, e218.
(38) Xie, B.; Tang, K.; Cheng, H.; Liu, Z.; Chen, S.; Tian, J. Coding acoustic metasurfaces. *Adv. Mater.* **2017**, *29*, 1503507.
(39) Xie, B. Y.; Cheng, H.; Tang, K.; Liu, Z. Y.; Chen, S. Q.; Tian, J. G. Multiband asymmetric transmission of airborne sound by coded metasurfaces. *Phys. Rev. Appl.* **2017**, *7*, 024010.
(40) Pu, M. B.; Zhao, Z. Y.; Wang, Y. Q.; Li, X.; Ma, X. L.; Hu, C. G.; Wang, C. T.; Huang, C.; Luo, X. G. Spatially and spectrally engineered spin-orbit interaction for achromatic virtual shaping. *Sci. Rep.* **2015**, *5*, 9822.
(41) Pu, M. B.; Li, X.; Ma, X. L.; Wang, Y. Q.; Zhao, Z. Y.; Wang, C. T.; Hu, C. G.; Gao, P.; Huang, C.; Ren, H. R. Catenary optics for achromatic generation of perfect optical angular momentum. *Science Advances* **2015**, *1*, e1500396.
(42) Xu, H. X.; Sun, S.; Tang, S.; Ma, S.; He, Q.; Wang, G. M.; Cai, T.; Li, H. P.; Zhou, L. Dynamical control on helicity of electromagnetic waves by tunable metasurfaces. *Sci. Rep.* **2016**, *6*, 27503.
(43) *H* plane is defined as the plane containing both the *H* field and wave-vector of the incident wave with linear polarization. For circularly polarized incident wave, *H* plane is defined as the plane containing the wave-vector and an arbitrary vector on the metasurface plane.
(44) Cheng, H.; Liu, Z.; Chen, S.; Tian, J. Emergent functionality and controllability in few-layer metasurfaces. *Adv. Mater.* **2015**, *27*, 5410−5421.
(45) Luo, W.; Sun, S.; Xu, H.; He, Q.; Zhou, L. Transmissive ultrathin Pancharatnam-Berry metasurfaces with nearly 100% efficiency. *Phys. Rev. Appl.* **2017**, *7*, 044033.

DOI: 10.1021/acsphotonics.7b01036
ACS Photonics 2018, 5, 1691−1702